PCCP

ROYAL SOCIETY OF CHEMISTRY

PAPER

View Article Online
View Journal

Cite this: DOI: 10.1039/d5cp04526f

Quantitative electronic structure determination of N-heterotriangulene derivatives adsorbed on Au(111)

Jakob Steidel,[a] Ina Michalsky,[b] Milan Kivala [b] and Petra Tegeder *[a]

Received 21st November 2025,
Accepted 9th February 2026

DOI: 10.1039/d5cp04526f

rsc.li/pccp

N-heterotriangulenes (N-HTAs) are promising organic semiconductors for applications in field effect transistors and solar cells. Thereby the electronic structure of organic/metal interfaces and thin films is essential for the performance of organic-molecule-based devices. Here, we studied the electronic properties of two different N-HTAs, the N-HTA-550 and N-HTA-557, the latter containing an additional 7-membered ring, adsorbed on Au(111) using two-photon photoemission spectroscopy. We quantitatively determined the energetic positions of several occupied and unoccupied molecular (transport levels) and excitonic states (optical gap) in detail. The additional –C═C– bridge forming the 7-membered ring in N-HTA-557 resulted in a pronounced increase of the electron affinity by 0.92 eV from 2.19 eV in N-HTA-550/Au(111) to 3.11 eV in N-HTA-557/Au(111) due to the increase of the π-conjugated electron system, while the first ionization potential is nearly unaffected. Structural variation or substitution pattern in N-HTAs foster the opportunity for tailoring their electronic properties.

1. Introduction

Organic semiconductors are potential candidates for many applications in (opto)electronic devices such as solar cells, light emitting diodes, or field effect transistors.[1–4] The electronic and adsorption properties of the organic compound at the interface to an inorganic electrode and within the molecular film are crucial for device performance. For instance, the orientation of molecules plays a central role for light absorption/emission and charge transport properties. Adsorbate/adsorbate and adsorbate/substrate interactions influence the adsorption geometry and the growth of molecular films, and accordingly, the electronic structure at the organic/inorganic interface (energy level alignment)[5–10] and within the molecular film.[11–18]

N-heteropolycyclic aromatic compounds are promising candidates for organic semiconductors as electron-transporting materials for use in field-effect transistors and solar cells.[19] The introduction of nitrogen atoms (pyridinic nitrogens) into the π-electron backbone of polycyclic aromatic hydrocarbons increases the electron affinity, *i.e.* the electron binding capability, while leaving the size of the optical gap nearly unaffected.[20–23] Pyrrolic nitrogens make the system more electron rich, that is lower the ionization potential.[24]

In the present contibution, we studied N-heterotriangulenes (N-HTAs, see Fig. 1), *ortho*-bridged triphenylamines,[24,25] which represent a class of functional molecules with high potential for application in optoelectronic materials,[26–29] for example as electron donating compounds in donor/acceptor systems.[30] Using structural variation (N-HTA-550 *vs.* -557) or substitution patterns opens the opportunity for fine-tuning the electronic properties.[24,27,31] Therefore, we recently analyzed the electronic properties and absorption spectra of two N-HTA derivatives, N-HTA-550 and N-HTA-557 (Fig. 1), at the interface to Au(111) and within thin molecular films using vibrational and electronic high resolution electron energy loss spectroscopy (HREELS) in combination with quantum chemical calculations. We found that the additional –C═C– bridge forming the 7-membered ring in N-HTA-557 resulted in a pronounced reduction of the

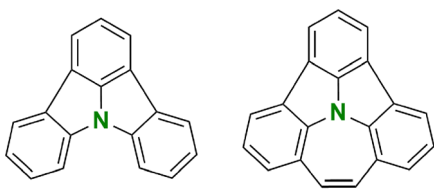

***N*-HTA-550** ***N*-HTA-557**

Fig. 1 The N-heterotriangulenes N-HTA-550 and N-HTA-557 investigated in the present study.

[a] *Physikalisch-Chemisches Institut, Ruprecht-Karls Universität Heidelberg, Im Neuenheimer Feld 253, 69120, Heidelberg, Germany. E-mail: tegeder@uni-heidelberg.de; Tel: +49 6221 548475*

[b] *Organisch-Chemisches Institut, Ruprecht-Karls Universität Heidelberg, Im Neuenheimer Feld 270, 69120, Heidelberg, Germany*

optical gap size by 0.9 eV from 3.4 eV in N-HTA-550 to 2.5 eV in N-HTA-557 due to an increase of the π-conjugated electron system.[32] Herein, we employed two-photon photoemission (2PPE) spectroscopy to determine quantitatively the energetic positions of unoccupied and occupied molecular electronic as well as excitonic states.

2PPE has been proven to be a powerful tool to elucidate the electronic structure of metal/organic interfaces and thin films. This includes electron affinity levels and ionization potentials (transport levels) as well as optical gaps and exciton binding energies.[33–54] Recently, we investigated the energy level alignment of a π-expanded N-heterotriangulene derivative adorbed on Au(111) by means of 2PPE and determined transport levels, the optical gap and accordingly the exciton binding energy.[54]

In the present contribution we thoroughly elucidated the electronic structure of N-HTA-550/Au(111) and N-HTA-557/Au(111) in detail, including the identification of transport levels, the optical gap and hence the exciton binding energy. In particular for applications of these materials in organic field effect transistors or solar cells knowledge about the energetic positions of transport levels is of utmost relevance.

2. Experimental details

The 2PPE experiments were performed under ultra-high vacuum (UHV, $< 2 \times 10^{-10}$ mbar) conditions at a sample temperature of around 90 K. The Au(111) single crystal was prepared by standard procedure of Ar^+ sputtering and annealing. The N-HTAs were synthesized according to the procedures reported in ref. 24. The compounds were deposited from an effusion cell held at 373 K for N-HTA-550 and at 393 K for N-HTA-557 onto the Au(111) sample held at 200 K for N-HTA-550 deposition and at 250 K in the case of N-HTA-557. The coverage was determined by temperature-programmed desorption (TPD) measurements (see below). 2PPE allows investigation of occupied, unoccupied electronic and excitonic states in a pump–probe scheme. To discriminate between occupied and unoccupied molecular electronic states photon-energy dependent measurements were performed as described in ref. 37,38,42–44. The tunable femtosecond laser system, which delivers laser pulses over a wide range of photon energies, and the 2PPE setup are described elsewhere.[55]

3. Results and discussion

To determine the adsorbate coverage and to analyze the adsorption behavior of the N-HTAs adsorbed on Au(111) we performed coverage-dependent TPD measurements. Fig. 2 shows TPD data for various initial N-HTA-550 (Fig. 2a) and N-HTA-557 (Fig. 2b) coverages. In the case of N-HTA-550/Au(111) three desorption features labeled as α_1, α_2, and α_3 are detected. α_1 shows a clear zero-order desorption characteristics (the desorption rate is independent of the coverage) and does not saturate even for higher coverages. Thus, α_1 can be assigned to the desorption from the multilayer. We attribute α_3 to

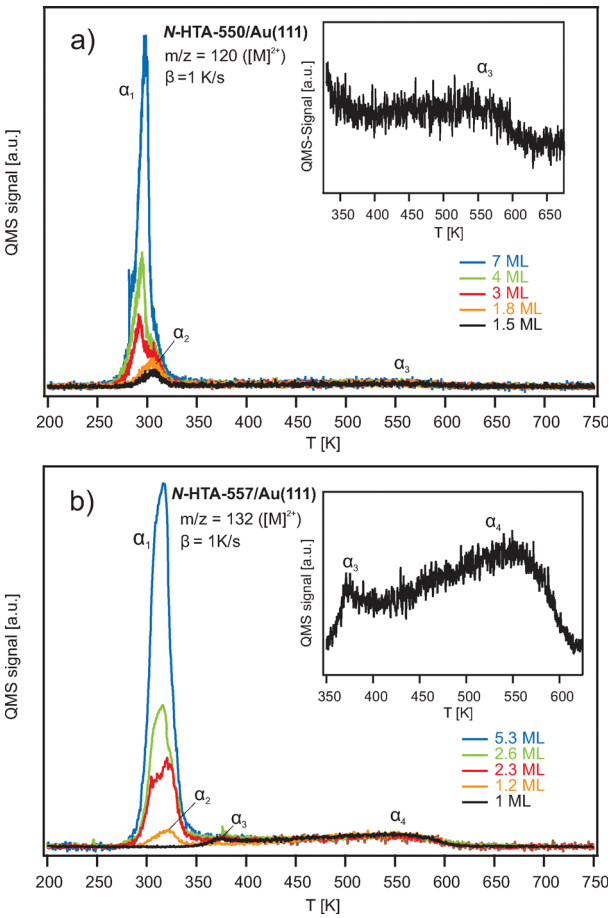

Fig. 2 Temperature-programmed desorption (TPD) spectra of (a) N-HTA-550 and (b) N-HTA-557 on Au(111) with different initial coverages recorded with a heating rate of β = 1 K s^{-1} at the fragment mass of m/z = 120 in the case of N-HTA-550 and m/z = 132 for N-HTA-557. The insets show the monolayer regime.

desorption from the monolayer and α_2 to the desorption from the second layer. We defined a monolayer (ML) to the desorption spectrum, in which α_3 is saturated. The integral of this spectrum is used as a reference to determine the coverage of all other TPD spectra shown in Fig. 2a. For N-HTA-557/Au(111) (Fig. 2b) α_1 is also assigned to the desorption from the multilayer, however it shows a first-order desorption characteristics rather than zero-order. As in the case of N-HTA-550 a desorption peak from the second layer (α_2) is observed. Apart from the monolayer desorption (α_4), a desorption feature labeled as α_3 is detected. We attribute α_3 to desorption from a more densely packed compressed phase, as reported for benzene[56,57] or other aromatic organic molecules on coinage metal surfaces.[41,58–63] Note that the peak area of α_4 has been used to define a coverage of 1 ML N-HTA-557/Au(111). Comparing both N-HTA/Au(111) systems, the desorption behavior in the multilayer regime (zero-order *vs.* first-order desorption) and in the low-coverage range (compressed phase) differs, indicating that the adsorbate–adsorbate (lateral) as well as the adsorbate–substrate (vertical) interactions are different. Consequently, we assume that the film morphology of the two systems differs.

To gain insight into the energy level alignment, *i.e.*, the energetic positions of adsorbate-derived occupied as well as unoccupied electronic states we performed photon-energy-dependent 2PPE measurements.[41–44,48,49,51,52,64] Fig. 3(a) shows an exemplarily 2PPE spectrum of 3 ML N-HTA-550 adsorbed on Au(111) recorded with $h\nu = 4.33$ eV (for additional 2PPE data see supplementary information (SI)). Several photoemission features could be detected some of them are related to the Au(111) surface such as the gold d-bands (at −2.15 eV and −2.74 eV with respect to Fermi energy (E_F) of the Au(111) surface) and the shifted surface state (SS′, at −0.22 eV) others are N-HTA-550-derived 2PPE peaks. On the basis of their photon-energy-dependency they are assigned to occupied and unoccupied molecular states as well as an excitonic state (see Fig. 3b). We detect three photoemission peaks in the photon energy-dependent spectra with a slope of around two, thus they are originating from occupied single-electron states. In the molecular orbital picture, these states can be assigned to the HOMO, HOMO−1 and HOMO−2, possessing binding energies with respect to E_F of −1.60 ± 0.16, −2.47 ± 0.15, and −3.71 ± 0.15 eV, respectively. Moreover, we find two peaks which scale linearly with incident photon energy. They stem from intermediate states located at 2.56 ± 0.14 eV and 1.56 ± 0.15 eV with respect to E_F. We attribute the states to an unoccupied single-electron state, which is well represented by the LUMO of N-HTA-550, and an higher lying electronic state (see below).

In Fig. 4(a), we summarize the level alignments with respect to the vacuum level. As discussed before,[42,43,48,65,66] depending on the excitation mechanism, 2PPE probes transport levels. Unoccupied single-electron states can be populated *via* an electron transfer from the metal substrate to the molecule creating a negative ion resonance and occupied single-electron states are ionized, creating a positive ion resonance. Thus, we obtain the electron affinities (EA) and the ionization potentials (IP) of the investigated N-HTA-550 molecule. In addition, in 2PPE also intramolecular electronic excitation is possible, which corresponds to exciton generation, *i.e.* formation of an electron–hole pair, in which the molecule remains overall neutral. The minimal energy required for this process is the optical gap (E_{opt}), which corresponds to the excitation energy of the lowest excited singlet state. E_{opt} is smaller than the difference between the lowest IP and the highest EA, which are according to Koopman's theorem given as the negative orbital energies of the HOMO and the LUMO. The so-called transport gap is given as E_{transp} = IP−EA. The difference between the transport gap and the optical gap corresponds to the exciton binding energy $E_{transp}-E_{opt} = E_B$.[36,67] Combining our results described above, we obtain a transport gap of 4.19 eV (IP = 6.38 ± 0.16 eV, EA = 2.19 ± 0.14 eV),

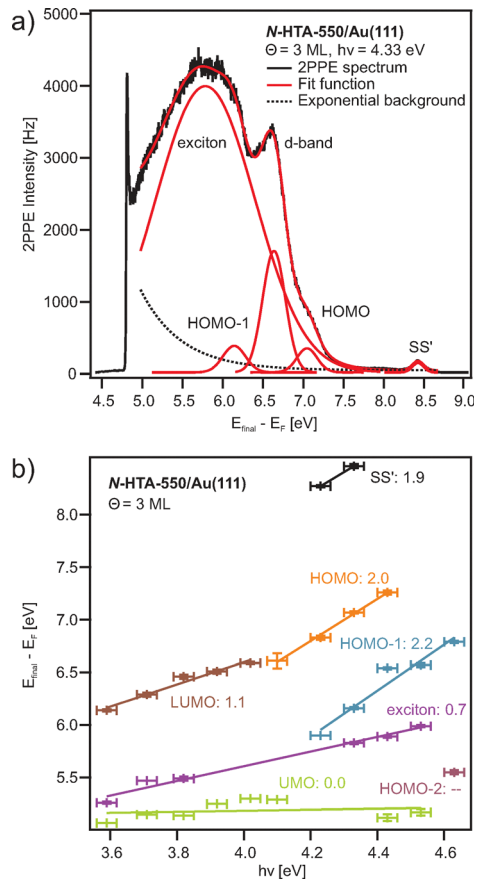

Fig. 3 (a) 2PPE spectrum of 3 ML N-HTA-550 adsorbed on Au(111). The data are fitted with an exponential background and Gaussian-shaped peaks (red curves). The energy axis reveals the final state (E_{Final}) of photoemitted electrons with respect to the Fermi energy E_F ($E_{Final} - E_F = E_{kin} + \Phi$); thus, the low-energy cutoff corresponds to the work function (Φ) of the adsorbate/substrate system. (b) Photon-energy-dependent peak position extracted to assign peaks observed in the 2PPE spectrum to occupied, unoccupied intermediate or final electronic states. A slope of 1 suggests that a peak originates from an unoccupied intermediate state, a slope of zero from an unoccupied final state (located above the vacuum level), while a slope of 2 is related to peaks originating from occupied states. The slopes from the fits are given next to the respective data.

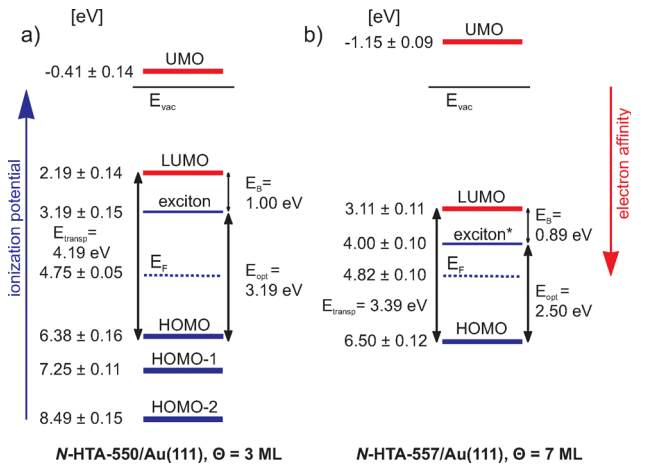

Fig. 4 (a) Energy level diagram of 3 ML N-HTA-550/Au(111) with respect to the vacuum level. The blue levels are the ionization potentials as well as an excitonic state and the red ones are the electron affinities, which are in the molecular orbital picture represented by the energies of the HOMOs, LUMO and UMO (unoccupied molecular orbital), respectively. E_F is the Au(111) Fermi level and E_{vac} is the vacuum level. (b) Energy level diagram of 7 ML N-HTA-557/Au(111). * denotes the value of the optical gap size determined by electronic HREELS from ref. 32.

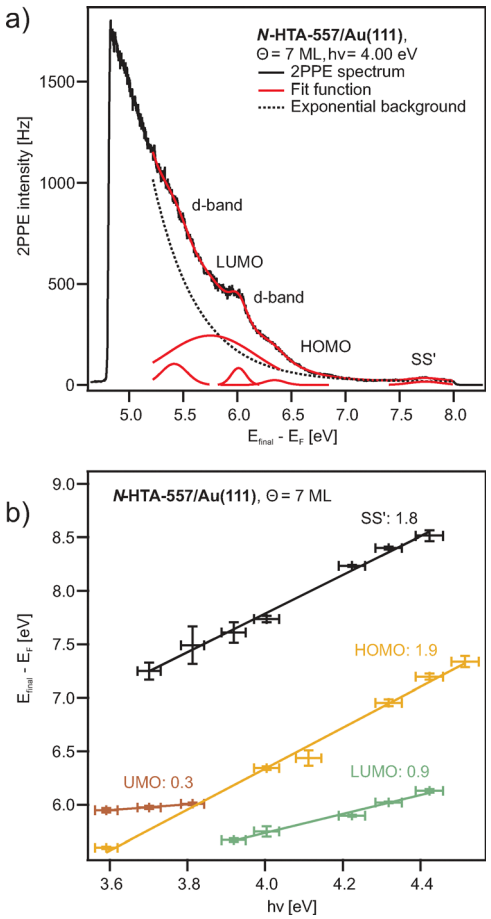

Fig. 5 (a) 2PPE spectrum of 7 ML N-HTA-557 adsorbed on Au(111). The data are fitted with an exponential background and Gaussian-shaped peaks (red curves). (b) Photon-energy-dependent peak position extracted to assign peaks observed in the 2PPE spectrum to occupied, unoccupied intermediate or final electronic states.

and an optical gap of 3.19 eV, the excitation energy of the lowest excited singlet state. Hence, E_B of the lowest excitonic state amounts to 1.0 eV. Note that with electronic HREELS measurements an optical gap of 3.4 eV has been determined,[32] thus 210 meV larger than the value obtained here. With this value the resulting exciton binding energy is 790 meV. Apart from the lowest IP, we determined two higher IPs corresponding to lower lying occupied single-electron states of N-HTA-550, which are described in the molecular orbital picture by the HOMO−1 and HOMO−2. In addition, we identified a further unoccupied molecular state (unoccupied molecular orbital: UMO) located 0.41 ± 0.14 eV above the vacuum level (E_{vac}, unoccupied final state).

Fig. 5(a) shows an exemplarily 2PPE spectrum of 7 ML N-HTA-557 adsorbed on Au(111) recorded with $h\nu$ = 4.0 eV (for additional 2PPE data see SI). Similar to the N-HTA-550/Au(111) system we detect photoemission features from the gold substrate (d-bands and SS′) but also adsorbate-induced 2PPE peaks. Based on their photon-energy-dependency they are assigned to the LUMO and HOMO as well as to an unoccupied final state (UMO) (see Fig. 5b). In Fig. 4(b), the level alignment with respect to the vacuum level is summarized. In comparison to N-HTA-550/Au(111) the 2PPE data for N-HTA-557/Au(111) are less structured, *i.e.* the photoemission signals are very broad and featureless. This is most likely related to the film morphology and surface roughness, which seems to be different in both systems (see above). Nevertheless the HOMO (IP) of N-HTA-557/Au(111) is located at 6.50 ± 0.12 eV and the LUMO (EA) at 3.11 ± 0.11 eV, resulting in a transport gap of 3.39 eV. Thus, the transport gap size decrease by 0.8 eV from 4.19 eV in N-HTA-550/Au(111) to 3.39 eV in N-HTA-557/Au(111), which is due to a pronounced increase of the EA by 0.92 eV as well as a slight rise of the IP by 120 meV in N-HTA-557/Au(111). Hence, the additional –C═C– bridge forming the 7-membered ring in N-HTA-557 which leads to an increase of the π-conjugated electron system strongly affects the EA level. Taking into account the optical gap size of 2.5 eV[32] measured with electronic HREELS would result in an exciton binding energy of 0.89 eV, which is similar to the value found for N-HTA-550/Au(111).

Concerning the organic/metal interface, we found for both systems a work function (Φ) decrease from 5.50 eV for the bare Au(111) surface to 4.8 eV at a coverage of 1 ML N-HTA/Au(111), thus a reduction of 700 meV (see Fig. S5 and S11). The reduction in work function can be explained by an induced interface dipole. For higher coverages Φ remains unchanged. For 1 ML N-HTA-550/Au(111) we observed 3 adsorbate-induced photoemission peaks (see Fig. S5 and S6), which can be assigned to the HOMO, HOMO−1 and an unoccupied final state (see Fig. S7). An excitonic state or photoemission related to the LUMO as detected for multilayer coverages are not found, most likely due to the strong electronic coupling between molecular electronic states and metallic band resulting in ultrashort lifetimes. For ≈1 ML N-HTA-557/Au(111) the resulting 2PPE data only resolve electronic states related to the Au(111) surface (see Fig. S11). Note that, no dispersing molecular states at the metal/organic interface of both systems have been observed in our angle-resolved 2PPE measurements, which for instance have been identified for other N-heteropolycycles adsorbed on Au(111).[51,52] Thus we exclude hybridization between the molecular states and metal bands.

4. Conclusion

Two N-heterotriangulene (N-HTA) derivatives, the N-HTA-550 and N-HTA-557 adsorbed on Au(111) have been investigated using energy-resolved two-photon photoemission (2PPE) spectroscopy, focusing on the quantitative determination of occupied and unoccupied molecular (transport states) and excitonic states (optical gap) as well as the influence of the –C═C– bridge and hence the formation of the 7-membered ring in N-HTA 557 on the electronic structure. For both compounds we were able to assign several 2PPE features to transport levels (electron affinities (EAs) and ionization potentials (IPs)) and excitonic states. Moreover exciton binding energies have been determined. The additional –C═C– bridge forming the 7-membered ring in N-HTA-557 which leads to an increase of the π-conjugated electron system strongly affected the first

EA level and resulted in a pronounced rise of the EA by 0.92 eV from 2.19 eV in N-HTA-550/Au(111) to 3.11 eV in N-HTA-557/Au(111). In contrast, the first IP is barely affected. Using structural variation or substitution pattern may pave the way for fine-tuning the electronic properties of N-HTAs at will.

Author contributions

J. S. performed the 2PPE measurements and analysed the results. I. M. synthesized the N-HTA derivatives. P. T. wrote the manuscript. M. K. supervised I. M. and P. T. supervised J. S. All authors reviewed the manuscript.

Conflicts of interest

The authors have no conflicts to declare.

Data availability

The data that support the findings of this study are available from the corresponding author upon request. Supplementary information (SI): two-photon photoemission data. See DOI: https://doi.org/10.1039/d5cp04526f.

Acknowledgements

Funding by the German Research Foundation (DFG) through the collaborative research center CRC 1249 ''N-Heteropolycycles as Functional Materials'' (Project Number 281029004-SFB 1249, Projects A05 and B06) is gratefully acknowledged.

References

1 S. Reineke, F. Lindner, G. Schwartz, N. Seidler, K. Walzer, B. Lüssem and K. Leo, *Nature*, 2009, **459**, 234.
2 B. W. D'Andrade and S. R. Forrest, *Adv. Mater.*, 2004, **16**, 1585–1595.
3 J. Lee, H. Chen, T. Batagoda, C. Coburn, P. I. Djurovich, M. E. Thompson and S. R. Forrest, *Nat. Mater.*, 2016, **15**, 92.
4 L. Torsi, M. Magliulo, K. Manoli and G. Palazzo, *Chem. Soc. Rev.*, 2013, **42**, 8612–8628.
5 H. Ishii, K. Sugiyama, E. Ito and K. Seki, *Adv. Mater.*, 1999, **11**, 605–625.
6 *The Molecule-Metal Interface*, ed. N. Koch, N. Ueno and A. Wee, Wiley-VCH, Weinheim, 2013.
7 M. Gruenewald, K. Wachter, M. Meissner, M. Kozlik, R. Forker and T. Fritz, *Org. Electron.*, 2013, **14**, 2177–2183.
8 S. Braun, W. R. Salaneck and M. Fahlman, *Adv. Mater.*, 2009, **21**, 1450–1472.
9 M. Oehzelt, N. Koch and G. Heimel, *Nat. Commun.*, 2014, **5**, 4174.
10 G. Mercurio, R. J. Maurer, W. Liu, S. Hagen, F. Leyssner, P. Tegeder, J. M. A. Tkatchenko, S. Soubatch, K. Reuter and F. S. Tautz, *Phys. Rev. B: Condens. Matter Mater. Phys.*, 2013, **88**, 035421.
11 J. L. Bredas, J. E. Norton, J. Cornil and V. Coropceanu, *Acc. Chem. Res.*, 2009, **42**, 1691–1699.
12 A. Köhler and H. Bässler, *Electronic Processes in Organic Semiconductors*, Wiley-VCH, Weinheim, Germany, 2015.
13 V. May and O. Kühn, *Charge and Energy Transfer Dynamics in Molecular Systems*, Wiley-VCH, Weinheim, Germany, 2011.
14 D. Beljonne, J. Cornil, L. Muccioli, C. Zannoni, J. L. Brédas and F. Castet, *Chem. Mater.*, 2011, **23**, 591–609.
15 V. Ruhle, A. Lukyanov, F. May, M. Schrader, T. Vehoff, J. Kirkpatrick, B. Baumeier and D. Andrienko, *J. Chem. Theory Comput.*, 2011, **7**, 3335–3345.
16 G. D'Avino, L. Muccioli, F. Castet, C. Poelking, D. Andrienko, Z. G. Soos, J. Cornil and D. Beljonne, *J. Phys.: Condens. Matter*, 2016, **28**, 433002.
17 M. B. Casu, *J. Electron Spectrosc. Relat. Phenom.*, 2015, **204**, 39–48.
18 R. Forker, M. Gruenewald and T. Fritz, *Annu. Rep. Prog. Chem., Sect. C: Phys. Chem.*, 2012, **108**, 34–68.
19 H. Klauk, U. Zschieschang, J. Pflaum and M. Halik, *Nature*, 2007, **445**, 745–748.
20 F. Würthner and M. Stolte, *Chem. Commun.*, 2011, **47**, 5109–5115.
21 U. H. F. Bunz, J. U. Engelhart, B. D. Lindner and M. Schaffroth, *Angew. Chem., Int. Ed.*, 2013, **52**, 3810–3821.
22 Q. Miao, *Adv. Mater.*, 2014, **26**, 5541–5549.
23 U. H. F. Bunz, *Acc. Chem. Res.*, 2015, **48**, 1676–1686.
24 I. Michalsky, V. Gensch, C. Walla, M. Hoffmann, F. Rominger, T. Oeser, P. Tegeder, A. Dreuw and M. Kivala, *Chem. – Eur. J.*, 2022, **28**, e202200326.
25 N. Hammer, T. A. Schaub, U. Meinhardt and M. Kivala, *Chem. Rec.*, 2015, **15**, 1119–1131.
26 U. Meinhardt, F. Lodermeyer, T. A. Schaub, A. Kunzmann, P. O. Dral, A. C. Sale, F. Hampel, D. M. Guldi, R. D. Costa and M. Kivala, *RSC Adv.*, 2016, **6**, 67372–67377.
27 M. Hirai, N. Tanaka, M. Sakai and S. Yamaguchi, *Chem. Rev.*, 2019, **119**, 8291–8331.
28 T. A. Schaub, K. Padberg and M. Kivala, *J. Phys. Org. Chem.*, 2020, **33**, e4022.
29 M. Krug, M. Wagner, T. A. Schaub, W. Zhang, C. M. Schüßlbauer, J. D. R. Ascherl, P. W. Münich, R. R. Schröder, F. Gröhn and P. O. Dral, *et al.*, *Angew. Chem., Int. Ed.*, 2020, **59**, 16233–16240.
30 M. Ajdari, R. Pappenberger, C. Walla, I. Michalsky, F. Maaß, M. Kivala, A. Dreuw and P. Tegeder, *J. Phys. Chem. C*, 2024, **128**, 14399–14406.
31 N. Deng and G. Zhang, *Org. Lett.*, 2019, **21**, 5248–5251.
32 M. Ajdari, R. Pappenberger, C. Walla, M. Hoffmann, I. Michalsky, M. Kivala, A. Dreuw and P. Tegeder, *J. Phys. Chem. C*, 2023, **127**, 542–549.
33 X.-Y. Zhu, *Surf. Sci. Rep.*, 2004, **56**, 1–83.
34 X.-Y. Zhu, *J. Phys. Chem. B*, 2004, **108**, 8778–8793.
35 C. Lindstrom and X.-Y. Zhu, *Chem. Rev.*, 2006, **106**, 4281–4300.
36 M. Muntwiler and X.-Y. Zhu, *Dynamics at Solid State Surfaces and Interfaces*, Wiley-VCH, 2010.
37 C. Bronner, M. Schulze, S. Hagen and P. Tegeder, *New J. Phys.*, 2012, **14**, 043023.

38 C. Bronner, G. Schulze, K. J. Franke, J. I. Pascual and P. Tegeder, *J. Phys.: Condens. Matter*, 2011, **23**, 484005.
39 N. Armbrust, J. Güdde, P. Jakob and U. Höfer, *Phys. Rev. Lett.*, 2012, **108**, 056801.
40 C. Bronner, S. Stremlau, M. Gille, F. Braußе, A. Haase, S. Hecht and P. Tegeder, *Angew. Chem., Int. Ed.*, 2013, **52**, 4422–4425.
41 C. Bronner, B. Priewisch, K. Rück-Braun and P. Tegeder, *J. Phys. Chem. C*, 2013, **117**, 27031–27038.
42 L. Bogner, Z. Yang, S. Baum, R. F. M. Corso, P. Bäuerle, K. J. Franke, J. I. Pascual and P. Tegeder, *J. Phys. Chem. C*, 2016, **120**, 27268–27275.
43 L. Bogner, Z. Yang, M. Corso, R. Fitzner, P. Bäuerle, K. J. Franke, J. I. Pascual and P. Tegeder, *Phys. Chem. Chem. Phys.*, 2015, **17**, 27118–27126.
44 A. Stein, F. Maass and P. Tegeder, *J. Phys. Chem. C*, 2017, **121**, 18075–18083.
45 D. Gerbert, F. Maass and P. Tegeder, *J. Phys. Chem. C*, 2017, **121**, 15696–15701.
46 D. Gerbert and P. Tegeder, *J. Phys. Chem. Lett.*, 2017, **8**, 4685–4690.
47 W. Bronsch, T. Wagner, S. Baum, M. Wansleben, K. Zielke, E. Ghanbari, M. Györök, A. Navarro-Quezada, P. Zeppenfeld and M. Weinelt, *et al.*, *J. Phys. Chem. C*, 2019, **123**, 7931–7939.
48 A. Stein, D. Rolf, C. Lotze, C. Czekelius, K. J. Franke and P. Tegeder, *J. Phys.: Condens. Matter*, 2019, **31**, 044002.
49 M. Ajdari, A. Stein, M. Hoffmann, M. Müller, U. H. F. Bunz, A. Dreuw and P. Tegeder, *J. Phys. Chem. C*, 2020, **124**, 7196–7204.
50 M. Ajdari, T. Schmitt, M. Hoffmann, F. Maass, H. Reiss, U. H. F. Bunz, A. Dreuw and P. Tegeder, *J. Phys. Chem. C*, 2020, **124**, 13196–13205.
51 A. Stein, D. Rolf, C. Lotze, B. Günther, L. H. Gade, K. J. Franke and P. Tegeder, *J. Phys. Chem. Lett.*, 2021, **12**, 947–951.
52 A. Stein, D. Rolf, C. Lotze, S. Feldmann, D. Gerbert, B. Günther, A. Jeindl, J. J. Cartus, O. T. Hofmann and L. H. Gade, *et al.*, *J. Phys. Chem. C*, 2021, **125**, 19969–19979.
53 K. Stallberg, A. Namgalies, S. Chatterjee and U. Höfer, *J. Phys. Chem. C*, 2022, **126**, 12728–12734.
54 J. Steidel, I. Michalsky, M. Ajdari, M. Kivala and P. Tegeder, *Phys. Chem. Chem. Phys.*, 2024, **26**, 16454–16458.
55 P. Tegeder, *J. Phys.: Condens. Matter*, 2012, **24**, 394001.
56 T. J. Rockey, M. Yang and H.-L. Dai, *J. Phys. Chem. B*, 2006, **110**, 19973–19978.
57 F. Maaß, Y. Jiang, W. Liu, A. Tkatchenko and P. Tegeder, *J. Chem. Phys.*, 2018, **148**, 214703.
58 M. Schulze, C. Bronner and P. Tegeder, *J. Phys.: Condens. Matter*, 2014, **26**, 355004.
59 S. Hagen, F. Leyssner, D. Nandi, M. Wolf and P. Tegeder, *Chem. Phys. Lett.*, 2007, **444**, 85–90.
60 P. Tegeder, S. Hagen, F. Leyssner, M. Peters, S. Hecht, T. Klamroth, P. Saalfrank and M. Wolf, *Appl. Phys. A: Mater. Sci. Process.*, 2007, **88**, 465–472.
61 E. R. McNellis, C. Bronner, J. Meyer, M. Weinelt, P. Tegeder and K. Reuter, *Phys. Chem. Chem. Phys.*, 2010, **12**, 6404–6412.
62 L. Óvári, Y. Luo, F. Leyssner, R. Haag, M. Wolf and P. Tegeder, *J. Chem. Phys.*, 2010, **133**, 044707.
63 C. Bronner and P. Tegeder, *New J. Phys.*, 2014, **16**, 053004.
64 C. Bronner, M. Schulze, S. Hagen and P. Tegeder, *New J. Phys.*, 2012, **14**, 043032.
65 E. Varene, I. Martin and P. Tegeder, *J. Phys. Chem. Lett.*, 2011, **2**, 252–256.
66 C. Bronner, D. Gerbert, A. Broska and P. Tegeder, *J. Phys. Chem. C*, 2016, **120**, 26168–26172.
67 M. Knupfer, *Appl. Phys. A: Mater. Sci. Process.*, 2003, **77**, 623–626.

